JBC RESEARCH ARTICLE

Methionine sulfoxide reductase 2 regulates Cvt autophagic pathway by altering the stability of Atg19 and Ape1 in *Saccharomyces cerevisiae*

Received for publication, October 3, 2023, and in revised form, December 31, 2023 Published, Papers in Press, January 20, 2024,
https://doi.org/10.1016/j.jbc.2024.105662

Arpan Chatterjee and Naresh Babu V. Sepuri*

From the Department of Biochemistry, School of Life Sciences, University of Hyderabad, Hyderabad, Telangana, India

Reviewed by members of the JBC Editorial Board. Edited by Ursula Jakob

The reversible oxidation of methionine plays a crucial role in redox regulation of proteins. Methionine oxidation in proteins causes major structural modifications that can destabilize and abrogate their function. The highly conserved methionine sulfoxide reductases protect proteins from oxidative damage by reducing their oxidized methionines, thus restoring their stability and function. Deletion or mutation in conserved methionine sulfoxide reductases leads to aging and several human neurological disorders and also reduces yeast growth on non-fermentable carbon sources. Despite their importance in human health, limited information about their physiological substrates in humans and yeast is available. For the first time, we show that Mxr2 interacts *in vivo* with two core proteins of the cytoplasm to vacuole targeting (Cvt) autophagy pathway, Atg19, and Ape1 in *Saccharomyces cerevisiae*. Deletion of *MXR2* induces instability and early turnover of immature Ape1 and Atg19 proteins and reduces the leucine aminopeptidase activity of Ape1 without affecting the maturation process of Ape1. Additonally, Mxr2 interacts with the immature Ape1, dependent on Met17 present within the propeptide of Ape1 as a single substitution mutation of Met17 to Leu abolishes this interaction. Importantly, Ape1 M17L mutant protein resists oxidative stress-induced degradation in WT and *mxr2*Δ cells. By identifying Atg19 and Ape1 as cytosolic substrates of Mxr2, our study maps the hitherto unexplored connection between Mxr2 and the Cvt autophagy pathway and sheds light on Mxr2-dependent oxidative regulation of the Cvt pathway.

Reactive oxygen species (ROS) act as a double-edged sword in the cell. At low concentrations, it manifests as a signaling molecule for growth and differentiation; however, uncontrolled accumulation causes oxidative stress. ROS-triggered oxidative stress impairs biomolecule function, leading to pathological conditions (1–5). Cells have evolved diverse strategies to combat oxidative insults, including enzymatic and nonenzymatic antioxidants (6). Sulfur-containing amino acids such as cysteine and methionine are the prime targets of ROS (7, 8). Methionine oxidation gives rise to reversible methionine sulfoxide (Met-SO) or irreversible methionine sulfenic acid (Met- SO2). Methionine sulfoxides obtain R or S enantiomeric forms that can be reduced by the canonical methionine sulfoxide reductases (MSRs), which are evolutionarily conserved from bacteria to humans (9–11). To prevent the accumulation of oxidized methionine, Msrs employ its native active cysteines to reduce methionine sulfoxides in the substrates (12–14). In reducing methionine sulfoxides, Msrs concomitantly get oxidized and are rendered inactive. However, the cell uses the thioredoxin and thioredoxin reductases to reduce and activate the Msrs, underscoring their importance in redox homeostasis (15, 16). Based on the type of enantiomeric form of the methionine sulfoxide that Msrs act on, Msrs are classified into A and B families. While members of the A family act on the Met-(S)-SO, the B family members act on the Met-(R)-SO (9). Yeast has three Msrs, Mxr1, Mxr2, and free methionine-(R)-sulfoxide reductase (fRMsr). Mxr1 belongs to the A family, while the latter belongs to the B family (17). Curiously, while Mxr1 and Mxr2 act on oxidized methionine in proteins, fRMsr works on free methionine (14, 18).

Loss or reduction in Msrs' activity has been implicated in many diseases, including pulmonary, vascular, ocular, aging, and neurological disorders (19–23). The known physiological consequences of dysfunctional Msrs are mitochondrial dysfunction, decreased cytochrome C biosynthesis, and metal resistance in yeast (17, 24). Given the dynamic nature of ROS levels, the importance of redox homeostasis, the alacrity at which the cells reactivate Msrs, the number of diseases associated with dysfunctional Msrs, and the plethora of proteins that harbor methionine, more studies are required to identify the substrates of Msrs rapidly and to unravel the ramifications of Msrs role that impinge on the structural and functional stability of proteins.

Cytoplasm to vacuole targeting (Cvt) pathway is a well-characterized selective autophagy pathway in yeast that delivers vacuolar hydrolases from the cytoplasm to the vacuolar lumen (25–27). Cvt vesicles are specialized autophagosomes which specifically enclose Cvt cargos and are much smaller (~150 nm) than starvation-induced autophagosomes (300 nm-900 nm) (25, 28). The vacuolar hydrolases that are transported *via* the Cvt pathway are leucine aminopeptidase (Ape1), α-mannosidase (Ams1), and aspartyl aminopeptidase (Ape4). Among the three hydrolases, Ape1 is the primary cargo and

* For correspondence: Naresh Babu V. Sepuri, nareshuohyd@gmail.com, nbvssl@uohyd.ernet.in.

forms the core of the Cvt vesicle. Ape1 is synthesized in the cytosol as an inactive zymogen (prApe1) harboring an N-terminal 45 amino acid propeptide. The propeptide of prApe1 mediates the intermolecular interaction of prApe1 molecules to create a homododecamer scaffolding structure that further congregates into the Ape1 complex that shapes the Cvt vesicle core (29, 30). The exposed first α-helical region of Ape1 propeptides in the Ape1 complex interacts with the adaptor protein, Atg19, to form a heterotrimer structure known as the Cvt complex (31–36). Ams1 and Ape4, the other two cargo of this pathway, are also associated with the Cvt complex *via* distinct interactions with Atg19 (37–40). The C-terminal region of Atg19 in the Cvt complex interacts with the master adaptor protein of selective autophagy, Atg11. With the help of the actin cytoskeleton and Arp2/3 actin binding complex, Atg11 facilitates the Cvt complex to reach the phagophore assembly site (PAS) (33, 41–43). After reaching PAS, Atg19 interacts with the Atg8 protein to form a β sheet structure, and this interaction tethers the Cvt complex with the phagophore and aids in phagophore expansion around the Cvt complex (44, 45). Vps53 tethering complex (VFT) also assists in localizing the Cvt complex and Atg19 in PAS (46).

Once properly localized at PAS, the VFT complex, Vps45, QSNAREs (Tlg1 and Tlg2), and the autophagy machinery drive the Cvt vesicle formation (47). After vesicle formation, Atg8 molecules attached to the outer surface of the Cvt vesicle are cleaved off by Atg4, and finally, the vesicle docks and fuses with the vacuole to release the inner single membrane compartment into the vacuolar lumen (48). Atg15 in the vacuolar lumen acts as a lipase to degrade the inner membrane, releasing Cvt vesicle cargo into the lumen (49, 50). In the lumen, Pep4 cleaves the propeptide of the Ape1, resulting in the formation iApe1 which further gets processed by Prb2 for maturation and activation of the Ape1 enzyme (51). At the same time, the other cargo hydrolases do not require processing as they do not have any propeptide (52). Cvt pathway has been extensively studied to identify the molecular players regulating it and as a model system to delineate selective autophagy pathways. However, little is known about the stability and turnover rate of the proteins orchestrating the intricate Cvt pathway under normal, oxidative, and nutrient stress conditions.

Our earlier study published identified the first substrate for Mxr2, Mge1, the nucleotide exchange factor for mitochondrial Hsp70 (53, 54). Recently, it has been shown that cytosolic Hsp40 may also be a probable substrate of Mxr2. Since Mxr2 is present in the cytosol and mitochondria, we wished to identify other cytosolic substrates of Mxr2. This study demonstrates Ape1 and Atg19 as potential substrates of Mxr2. Compared to the control condition, both proteins exhibit enhanced turnover rates under oxidative stress or without Mxr2. Further, we have identified a methionine residue in the Ape1 protein, M17, that is pivotal in interacting with Mxr2. This result is further bolstered by the finding that substitution mutation of M17 renders the Ape1 protein immune to oxidative stress and degradation. This study extends the substrate repertoire of Mxr2 by acting on critical proteins of the Cvt pathway apart from Mge1 and Hsp40.

Results

Mxr2 interacts with Ape1 and Atg19 of the Cvt pathway

To identify potential cytosolic substrates of Mxr2, we studied the high throughput data of yeast interactome. The data predicted Atg19 and Ape1 of the Cvt pathway to be probable substrates of Mxr2 (55). To validate this finding, a yeast two-hybrid assay was performed as described in the Experimental procedures. We find that Mxr2 strongly interacts with Atg19 and weakly with Ape1 as transformants carrying *MXR2* with *APE1* constructs cannot grow on the SC-Leu-Trp-Ade medium plate (Fig. 1*A*). To further confirm these interactions, we overexpressed *MXR2* with a 3x FLAG tag from the p426 vector and *ATG19* or *APE1* with a hemagglutinin (HA) tag from the p425 vector under the TEF1 promoter in *mxr2*Δ strain. Next, immunoprecipitation with FLAG antibody was carried out after growing the above strains as described in the Experimental procedures and the specificity of HA and FLAG antibodies as described (Supporting information 1). Immunoprecipitation results showed that Atg19 and Ape1 proteins interact with Mxr2 *in vivo.* To confirm the specificity of Mxr2 interaction with Atg19 and Ape1, we included Mxr1, which acts on S-methionine sulfoxide in the yeast two-hybrid assay. Unlike Mxr2, Mxr1 does not interact with Atg19 or Ape1 (Fig. 1*C*). Based on yeast two-hybrid and immunoprecipitation results, we show that Mxr2 interacts specifically with Atg19 and Ape1, which are crucial components of the Cvt pathway.

Mxr2 protects Ape1 and Atg19 proteins from oxidative stress and premature degradation

To gain insights into the physiological role of Mxr2 in the context of the Cvt pathway, we initially looked at whether Mxr2 affects prApe1 maturation. To investigate this, an Ape1 maturation assay was performed in wt, *mxr2*Δ, and *atg19*Δ strains under normal and nitrogen starvation conditions as described in the Experimental procedures. Strains were grown to the mid-log phase before being exposed to nitrogen starvation for 0 or 4 h. Next, cells were lysed, and lysates resolved on SDS-PAGE, Western transferred and immunoblotted with anti-Ape1 antibody. The specificity of the Ape1 antibody is confirmed by immunoblotting the wt and *ape1*Δ cell lysates (Supporting information 1). Immunoblotting results showed two distinct bands of molecular weights, 62 kDa and 50 kDa, corresponding to the prApe1 and mature Ape1 (mApe1) in the wt control strain (Fig. 2*A*i). As expected, the expression of Ape1 increased upon nitrogen starvation in the wt strain (Fig. 2*A*i) (56). In the absence of Atg19, maturation of Ape1 is abolished in control and nitrogen-starved cells (Fig. 2*A*i).

Intriguingly, the deletion of *MXR2* does not affect the maturation process of Ape1. However, the Ape1 protein level is significantly reduced compared to wt cells in control and nitrogen-starved cells (Fig. 2*A*i). As we observed the interaction of Mxr2 and ATG19 along with Ape1, we also looked at the expression of HA-tagged Atg19 in wt and *mxr2*Δ strains (Fig. 2*A*ii). As speculated, the protein expression of HA-Atg19

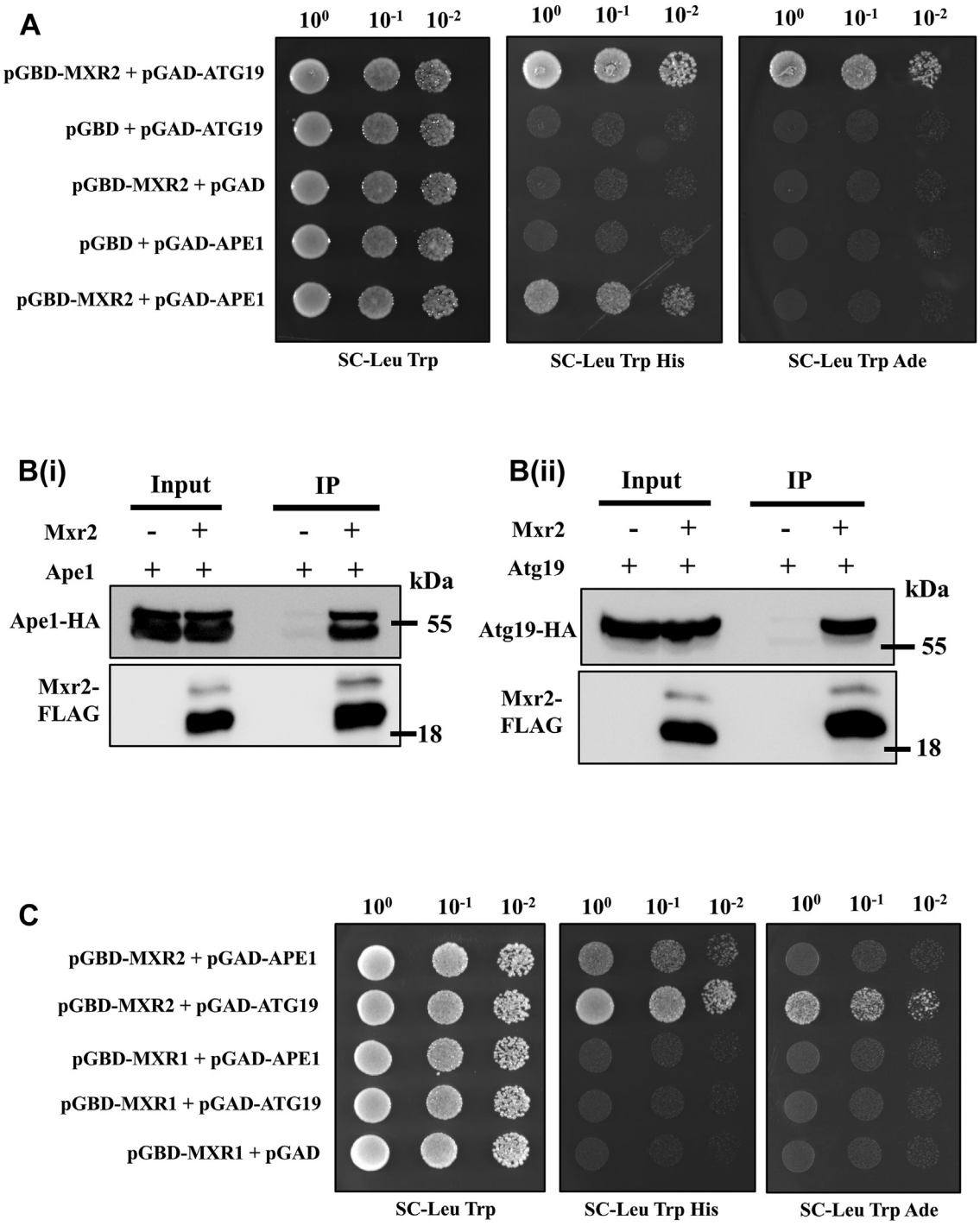

Figure 1. Mxr2 interacts with the Cvt pathway proteins, Atg19 and Ape1. *A*, yeast two-hybrid assay was performed between Mxr2 and Atg19 or Ape1. The PJ69-4A strain was transformed with pGBD-C1 (expressing *MXR2*) and pGAD-C1 (expressing *APE1* or *ATG19*) plasmids. Transformants were then grown in the presence and absence of histidine and adenine at 30 °C for 2 days. *B*(i), coimmunoprecipitation assay between Mxr2 and Ape1 (ii) coimmunoprecipitation assay between Mxr2 and Atg19. *mxr2*Δ cells expressing Mxr2-FLAG and either Ape1-HA or Atg19-HA were grown in a minimal medium lacking leucine and uracil up to the mid-log phase. *mxr2*Δ cells not expressing Mxr2 were kept as the negative control. Ape1-HA and Atg19-HA proteins were immunoprecipitated with anti-FLAG antibody. Western blotting was performed using anti-FLAG and anti-HA antibodies. *C*, yeast two-hybrid assay between Mxr1 and Atg19 or Ape1. The PJ69-4A strain was transformed with pGBD-C1 and pGAD-C1 constructs expressing Mxr1 and Atg19 or Ape1, respectively. For positive control in the assay, the PJ69-4A strain was transformed with pGBD-C1 expressing Mxr2 and pGAD-C1 expressing Ape1 or Atg19 and used. Transformants were then spotted in the same selection plates and grown at 30 °C for 2 days. Spotting assay and the immunoprecipitation experiments were performed twice. Full length blots are represented in Supporting information 1. Cvt, cytoplasm to vacuole targeting; HA, hemagglutinin.

from the pRS313 vector shows a modest decrease in *mxr2*Δ than the wt strain (Fig. 2*A*ii).

The apparent decrease in protein levels of Ape1 and Atg19 could be a cascading effect of a decline in their transcription. To determine if this is true, we examined the transcript levels of *APE1* and *ATG19* after isolating total RNA from wt and *mxr2*Δ strains. Quantitative reverse transcription PCR (qRT-PCR) results revealed no significant difference in the mRNA

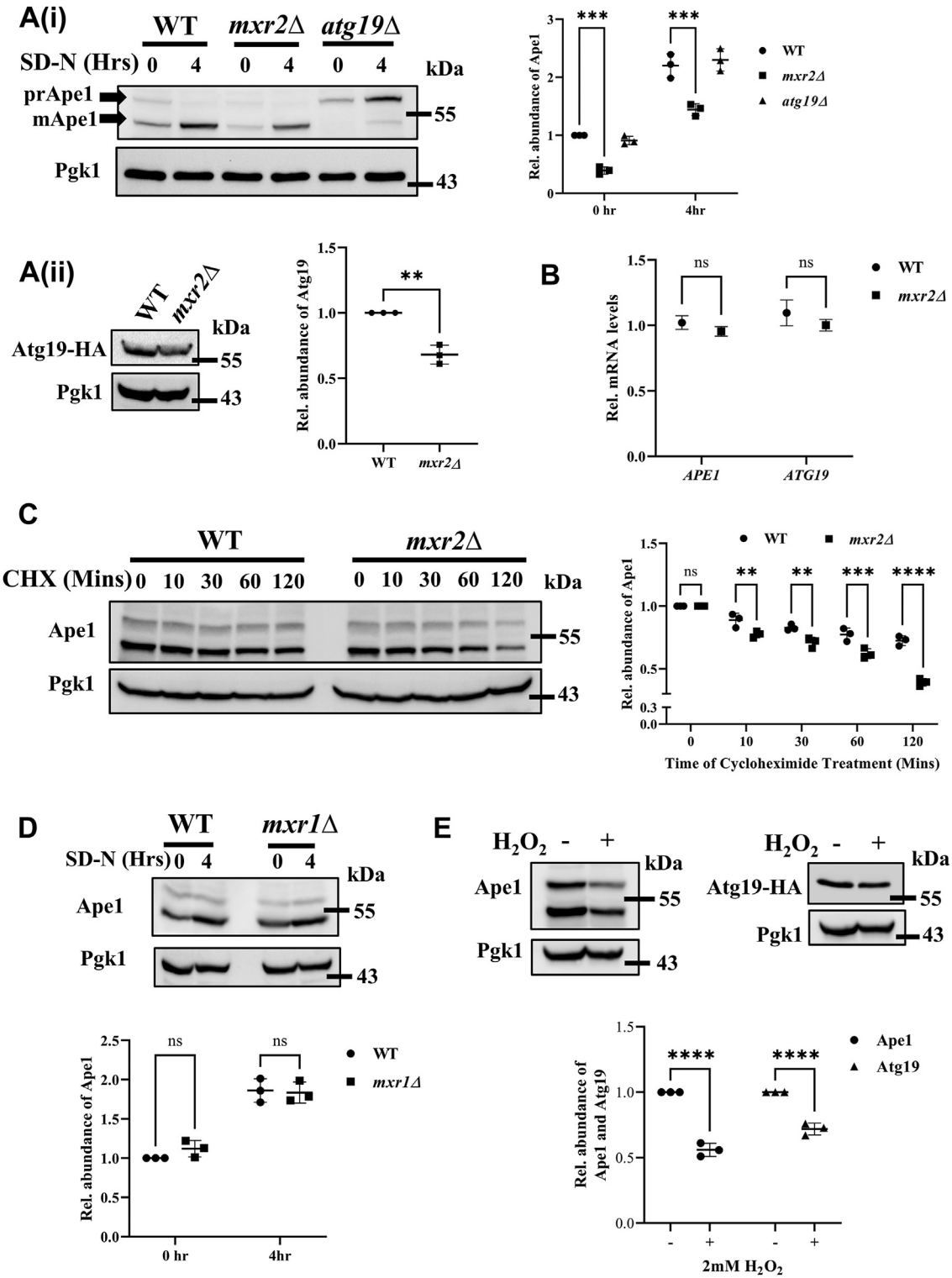

Figure 2. Mxr2 protects Ape1 and Atg19 proteins from oxidative stress-mediated degradation. *A*, analysis of the steady-state level of (i) the Ape1 protein in wt, *mxr2*Δ, and *atg19*Δ and (ii) the Atg19 protein in wt and *mxr2*Δ strains. For (i) wt, *mxr2*Δ, and *atg19*Δ strains were grown and then either left untreated or exposed to nitrogen starvation for 4 h, whereas for (ii) wt and *mxr2*Δ strains transformed with Atg19-HA CEN constructs and grown up to mid-log phase. Harvested cells were analyzed *via* Western blotting using either anti-Ape1 antibody (i) or anti-HA antibody (ii). *B*, *APE1* and *ATG19* transcript levels were checked in wt and *mxr2*Δ strains *via* qRT-PCR analysis. *C*, cycloheximide chase assay. wt and *mxr2*Δ strains were grown up to mid-log phase and treated with 50 μg of cycloheximide for 2 h, and then the Ape1 turnover profile was checked *via* Western blotting with anti-Ape1 antibody. *D*, wt and *mxr1*Δ strains were grown and left untreated or exposed to nitrogen starvation for 4 h. The steady-state level of Ape1 protein was checked in these conditions *via* Western blotting. *E*, degradation of the Ape1 protein under oxidative stress. wt strain was treated with 2 mM H_2O_2 for 2 h. Treated and untreated cells were analyzed for steady-state levels of Ape1 and Atg19 *via* Western blot. To monitor the Atg19 steady-state level, wt strain transformed with the CEN construct of Atg19-HA was used. The data shown are the mean ± SD of three biologically independent experiments and full-length blots are represented in supporting information 1. Statistical analysis was done using an unpaired Student's *t* test for (*B*), whereas for (*A*) and from (*C–E*), it was done using a two-way ANOVA test. ****$p < 0.0001$, ***$p < 0.001$, **$p < 0.01$ and *$p < 0.05$. ns, nonsignificant. HA, hemagglutinin; qRT-PCR; quantitative reverse transcription PCR.

levels of both genes in *the mxr2*Δ strain compared to the wt strain (Fig. 2*B*).

Considering the above results, we hypothesized that Mxr2 protects Ape1 and Atg19 from oxidative stress and degradation. To test this hypothesis, the turnover rate of Ape1 was monitored in wt and *mxr2*Δ strains. Cells were grown to the mid-log phase before treating them with cycloheximide for 2 h to stop the translation of new proteins. Temporal protein degradation monitoring was done by regularly harvesting cells during cycloheximide treatment. Western blotting was carried out on harvested cells as described above and in the Experimental procedures. The blots were probed with Ape1 and Pgk1 antibodies, the latter as a loading control (Fig. 2*C* and Supporting information 1). At zero time points, the Ape1 protein levels in both strains appear comparable (Fig. 2*C*). However, at the end of 2 h, the *mxr2*Δ strain significantly deviates from the wt strain as the Ape1 protein undergoes almost 60% degradation compared to 20 to 25% in the wt strain (Fig. 2*C*). Our results demonstrate that in the absence of Mxr2, the Ape1 protein is susceptible to premature degradation. To ensure that the protective function of Mxr2 on Ape1 is not a generic function of all MSRs, we monitored the steady-state levels of Ape1 in wt and *mxr1*Δ strains under nitrogen starvation, as described earlier. In contrast to the decreased level of Ape1 in *mxr2*Δ strain compared to WT strain under nitrogen starvation duress (Fig. 2*A*i), there is no change in Ape1 level in *mxr1*Δ strain (Fig. 2*D*). This result underscores the specificity of Mxr2 action on Ape1.

Our previous study (51) found excess ROS in the *mxr2*Δ strain compared to the wt strain. If the ROS-triggered antioxidant function of Mxr2 is driving its protective function on Ape1 and Atg19, increased oxidative stress should also affect the stability of these proteins. To ascertain if this assumption is accurate, we first treated wt strain expressing HA-Atg19 with 2 mM H_2O_2 for 2 h to induce the production of ROS. After that, we checked for the protein levels of Ape1 and HA-Atg19 by Western blotting (Fig. 2*E*). H_2O_2 treatment led to a significant reduction in the steady-state level of both proteins (Fig. 2*E*). The above results suggest that Mxr2 protects Ape1 and Atg19 from oxidative stress and premature degradation.

Amino acid methionine 17 in Ape1 is required for interaction with Mxr2

Yeast Ape1 exists in two intracellular protein pools, prApe1 and mApe1. The N-terminal 45 amino acid propeptide is cleaved by Pep4 protease in the vacuole to generate a 55 kDa intermediate form (iApe1) before being finally converted into the 50 kDa mature form (mApe1) by proteinase B (PRB1) (57). Yeast two-hybrid (Fig. 1*A*) and immunoprecipitation (Fig. 1*B*i) assays show that Mxr2 can interact with prApe1. To determine if Mxr2 can also interact with vacuolar processed Ape1 by yeast two-hybrid, we first amplified the Ape1 without the propeptide resembling the iApe1 (Ape1Δ 2–45aa) and cloned it into the pGAD-C1 vector as described in the Experimental procedures. Yeast two-hybrid was performed, and we observe that Mxr2 interacts with full-length Ape1 (prApe1) (Fig. 3*A*), as observed above (Fig. 1*A*); however, it fails to interact with iApe1 implying that the propeptide is essential for Mxr2 to interact with Ape1.

Mxr2 binds to oxidized methionine residues in the proteins to reduce them (58). Our earlier study (52) showed that Mxr2 interacts with Mge1 in a manner that is dependent on methionine 155, as substitution of methionine with leucine at 155 in Mge1 abolishes the interaction. Ape1 contains a total of six methionine residues, of which two are present in the propeptide (M1 and M17), and the remaining four are present in the mature peptide (M277, M312, M420, and M478). Since mApe1 does not interact with the Mxr2, we hypothesized that the association of Mxr2 with prApe1 may depend on M1 or M17 or both residues in Ape1. Site-directed mutagenesis generated three prApe1 constructs in the pGAD-C1 vector where M1, M17, or both (DM) were substituted with leucine for yeast two-hybrid studies. Both wt prApe1 and prApe1 M1L interact with Mxr2 (Fig. 3*B*). Strikingly, neither prApe1 M17L nor prApe1 M1L M17L exhibited any interaction with Mxr2 (Fig. 3*B*). To further confirm this result, we performed coimmunoprecipitation. First, we constructed plasmids that expressed *APE1* wt or *APE1* M17L mutant under its native promoter. Next, *the ape1*Δ strain was transformed with wt *APE1* or *APE1* M17L plasmid and the plasmid expressing FLAG-*MXR2* under the TEF1 promoter. Coimmunoprecipitation was carried out using the FLAG antibody as described in the Experimental procedures (Fig. 3*C*). WT Ape1 coprecipitates with FLAG-Mxr2, whereas the M17L mutant does not. Significantly, only the premature form of Ape1, not the mature form, precipitates with FLAG-Mxr2. These results reinforce the pivotal role of M17 in prApe1 interaction with Mxr2.

M17L mutation confers increased stability to Ape1

Oxidative stress triggers methionine oxidation in proteins, making them dysfunctional and vulnerable to degradation. Mxr2 has the innate ability to recognize oxidized methionine within proteins, bind, and reduce it. Counter-intuitively, we speculated what would happen if the methionine is mutated into an amino acid that cannot be oxidized. The protein will probably be insensitive to oxidative stress and become stable, and Mxr2 will not interact with the protein. If this is true, we reasoned that Ape1 M17L should resist oxidative stress and be highly stable. We expressed wt or M17L Ape1 protein from a pRS315 vector in *ape1*Δ and *ape1*Δ*mxr2*Δ strains to validate this thinking. The steady-state level of Ape1 protein was assessed as described earlier by immunoblotting with Ape1 antibody after exposure to 0 or 2 h of nitrogen starvation. Similar to earlier results (Fig. 2*A*i), the steady-state level of wt Ape1is reduced in the *ape1*Δ*mxr2*Δ strain in comparison to the *ape1*Δ strain (Fig. 4*A*), reinforcing the impact Mxr2 has on the stability of Ape1. Consistent with our reasoning, the Ape1 M17L mutant is highly stable as it is present at a significantly higher concentration than wt Ape1 with or without nitrogen starvation and in both strains (Fig. 4*A*). Deletion of *MXR2* does not affect the stability of Ape1 M17L (Fig. 4*A*). Ape1 M17L appears immune to oxidative stress and degradation.

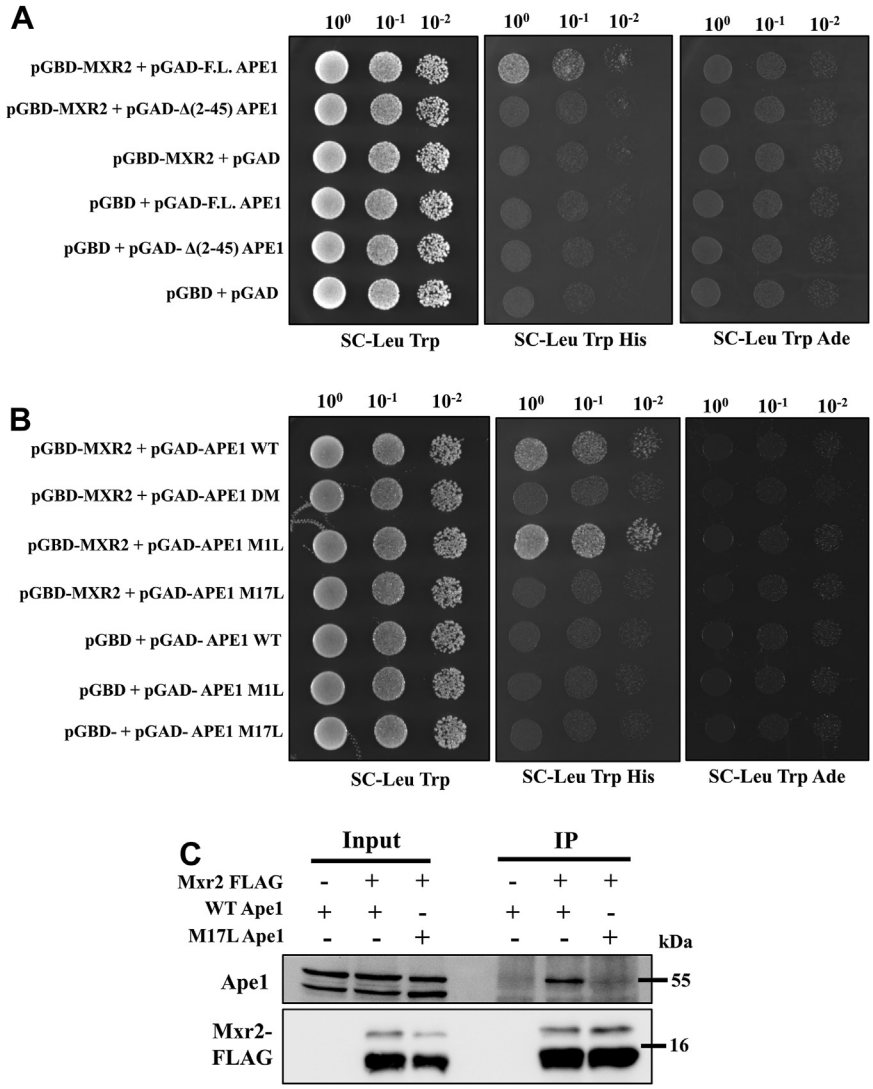

Figure 3. Mxr2 interacts exclusively with M17 residue of Ape1. *A*, yeast two-hybrid experiment between Mxr2 and either full-length or Δ (2–45aa) Ape1 constructs was carried out. The PJ69-4A strain was transformed with yeast two-hybrid vector constructs expressing indicated proteins. *B*, yeast two-hybrid experiment between Mxr2 and different methionine mutant constructs (M1L; M17L; M1L, M17L) of Ape1. *C*, coimmunoprecipitation assay between Mxr2 and wt or M17L mutant Ape1. *mxr2Δape1Δ* cells expressing Mxr2-FLAG and either wt or M17L Ape1 were grown up to the mid-log phase. The *mxr2Δape1Δ* cells transformed with wt Ape1 alone were used as a negative control. The anti-FLAG antibody was used to precipitate the Ape1 protein. Immunoprecipitated proteins were then detected *via* Western blots using anti-Ape1 and anti-FLAG antibodies. Spotting assay and the immunoprecipitation experiments were conducted twice and full-length blots are represented in Supporting information 2.

To rule out the possibility of increased expression of Ape1 M17L compared to wt Ape1, we isolated total RNA from cells expressing wt and Ape1 M17L and measured their transcription levels. The transcription of both genes is comparable, and no significant difference is observed (Fig. 4*B*). To verify that Ape1 M17L is less prone to turnover and thereby more stable, we performed the cycloheximide chase assay on *ape1Δ* cells expressing either wt or M17L mutant Ape1. We observe nearly 45 to 50% wt Ape1 protein degradation at the end of 2 h (Fig. 4*C*). Significantly and in contrast, Ape1 M17L is robust by displaying a mere 10% degradation (Fig. 4*C*).

mxr2Δ strain exhibits decreased LAP activity

Ape1 is a vacuolar resident leucine aminopeptidase (LAP), which cleaves N-terminal leucine residues. The enzyme is a member of the M18 class of zinc metalloproteases (59–61). *Saccharomyces cerevisiae* has four leucine aminopeptidases: Lap1/Ape2, Lap2, Lap3, and Lap4/Ape1 (61). As the deletion of *MXR2* affected the stability of Ape1, we reasoned that it may additionally affect its activity. To check this, we carried out the LAP activity assay. As the yeast cell harbors redundant LAPs, we measured the LAP activity in three strains, wt, *mxr2Δ*, and *ape1Δ* strains. Generally, leucine-β-naphthylamide or leucine-para-nitroanilide are used as substrates to assess the LAP activity. Both substrates generate fluorescent products after the reaction, which can be monitored in a spectrophotometer. Trumbly J. R. *et al.* showed that leucine-para-naphthylamide is the preferred substrate for Ape1 as it exhibits more activity with this substrate over the others (61, 62). Hence, we used leucine-para-naphthylamide as the substrate in our assays, as described in the Experimental procedures. Cell lysates from the

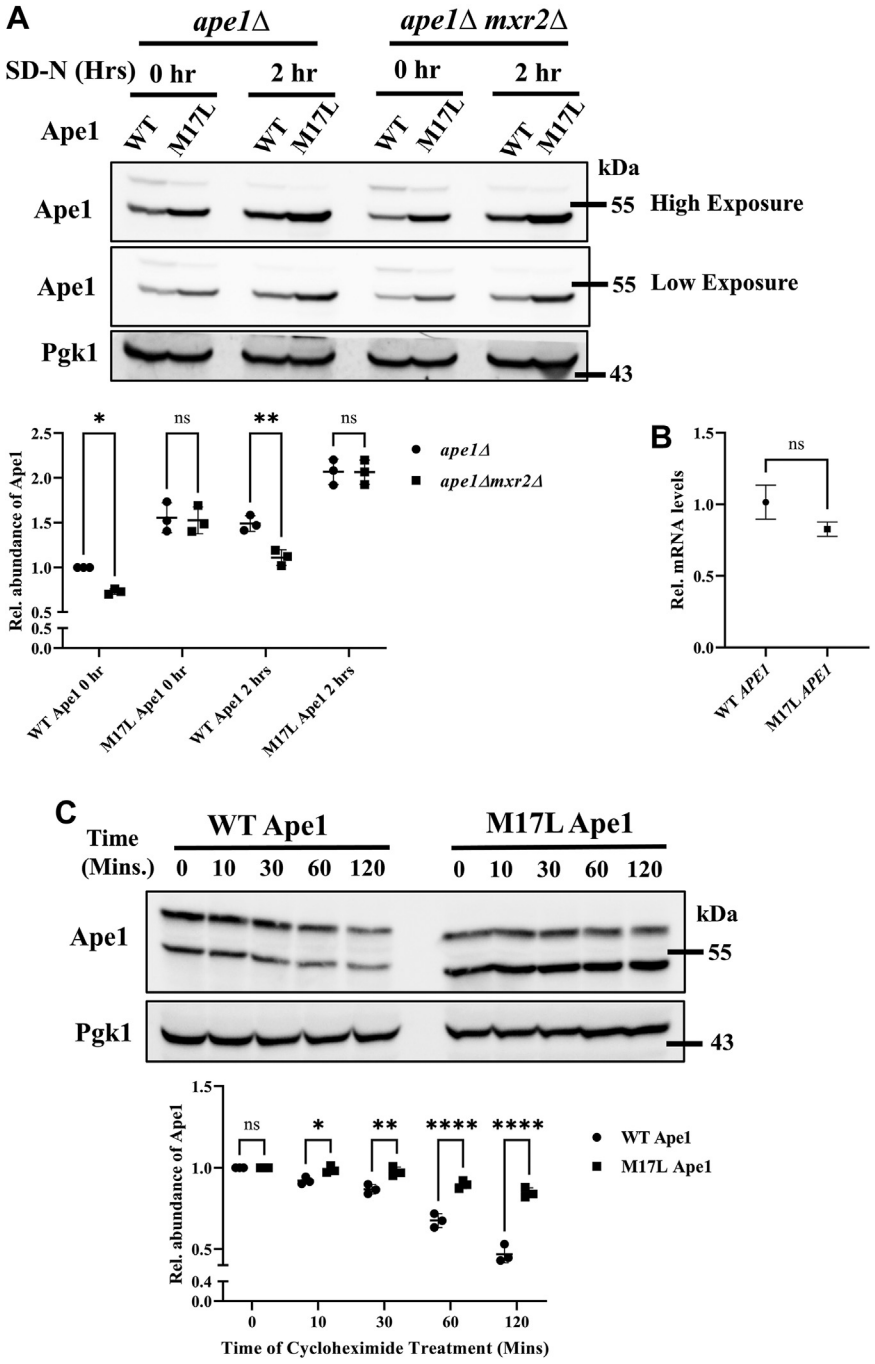

Figure 4. M17L mutant Ape1 resists degradation. *A*, *ape1*Δ and *ape1*Δ*mxr2*Δ strains expressing either wt or M17L mutant Ape1 were grown up to mid-log phase and further exposed to nitrogen starvation for 2 h or left untreated. Harvested cells were lysed and analyzed *via* Western blot. *B*, wt and M17L mutant Ape1 expressing cells were assessed to check the transcript level of Ape1. *C*, cells harboring wt and M17L Ape1 were grown and subjected to cycloheximide treatment for five different time points for up to 2 h. Harvested cells were analyzed *via* Western blot. Data is represented as mean ± SD of three independent experiments and full length blots are represented in Supporting information 2. Statistical analysis was done using an unpaired Student's *t* test for (*B*), whereas for (*A* and *C*), it was done using a two-way ANOVA test. ****$p < 0.0001$, ***$p < 0.001$, **$p < 0.01$ and *$p < 0.05$. ns, nonsignificant.

above three strains were used to perform the aminopeptidase assay, where μmol of product formed/mg of cell lysate was measured as described (Fig. 5*A*). The amount of product formed in the *mxr2*Δ strain is comparable to that in *the ape1*Δ strain; however, it is significantly lower than the wt strain (Fig. 5*B*). These results imply that the Ape1 enzyme molecules in *mxr2*Δ are oxidatively modified and less active.

Mxr2 helps in maintaining the stoichiometry of Ape1 and Atg19 in Cvt pathway

After the Ape1 complex formation, Atg19 interacts with Ape1, facilitating communication and association with other Atg proteins, including Atg8 and Atg11, to form Cvt vesicles. Considering the above information, we inquired whether overexpression of Atg19 alone or with Mxr2 can rescue the

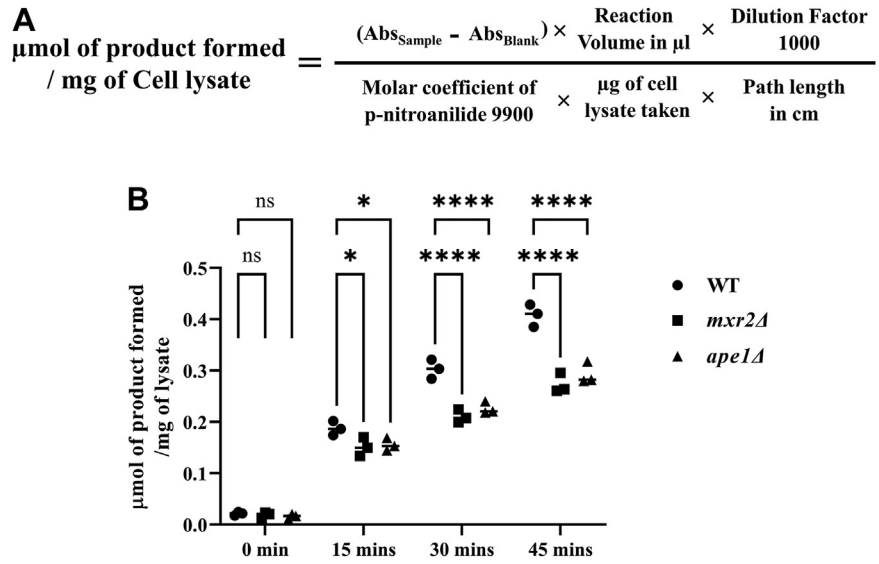

Figure 5. Leucine aminopeptidase activity decreases in *Δmxr2* strain. *A*, equation to estimate amount (µmol) of product formed/mg of lysate in leucine aminopeptidase assay. *B*, wt, *mxr2Δ* and *ape1*Δ cells were grown up to log phase, and cells lysates were prepared to check the leucine aminopeptidase activity of the cells. Fifty micrograms lysate from each strain was then incubated with leucine p-nitroanilide substrate for up to 45 min as described under methods. Samples were analyzed in a spectrophotometer by measuring their absorbance at 405 nm, and µmol of product formed was calculated for the three strains. Data are represented as mean ± SD of three independent experiments. Statistical analysis was done using a two-way ANOVA test. ****$p <$ 0.0001, ***$p < 0.001$, **$p < 0.01$ and *$p < 0.05$. ns, nonsignificant.

unstable phenotype of Ape1 in *the mxr2*Δ strain. HA-tagged *ATG19* plasmid alone or with FLAG-tagged *MXR2* plasmid were overexpressed in wt and *mxr2*Δ strains. The strains were grown until the mid-log phase before being exposed to nitrogen starvation for 4 h. As described earlier, cells were harvested, Western blotted, and probed with Ape1, HA, FLAG, and Pgk1 (loading control) antibodies (Fig. 6). Intriguingly, instead of rescuing the instability phenotype of Ape1, overexpression of Atg19 exacerbates the phenotype in not only *the mxr2*Δ strain but also destabilizes Ape1 in the wt strain (Fig. 6). This could be due to imbalanced stoichiometry of both the protein in the system. This effect is observed under normal physiological and nitrogen starvation conditions (Fig. 6). Interestingly, additional overexpression of Mxr2 does not improve the stability of Ape1 in wt or *mxr2*Δ strain under physiological conditions (Fig. 6). Strikingly, under nitrogen stress, Mxr2 overexpression restores the steady-state level of Ape1 in wt and *mxr2*Δ strains to that observed in wt cells transformed with an empty vector (Fig. 6). Moreover, Ape1 in *the mxr2*Δ strain exhibits increased stability in the presence of Mxr2 overexpression (Fig. 6). We conclude that Mxr2 acts as a shield protecting Ape1 and Atg19 from premature degradation during oxidative stress and thus maintains their stoichiometry for proper functioning of the Cvt pathway.

Discussion

ROS has been implicated in numerous signaling pathways that modulate developmental stages in different organisms. ROS has been noted to be involved in regulating ion channels and transporters, kinases and phosphatases, metabolic enzymes, G protein–coupled receptors, cytoskeletal elements, transcription factors, cell-cycle control factors, proteases, and chromatin-modifying enzymes (1). However, excess ROS generates oxidative stress that has deleterious consequences on proteins, DNA, lipids, and other biomolecules. Some detrimental effects include mutations, enzyme inactivity, cytotoxicity, physiological abnormalities, and pathological conditions (63). Of all the amino acids, sulfur-containing amino acids methionine and cysteine are the most vulnerable to oxidation. Oxidative stress induces a disulfide link between two cysteines to form a cystine.

In contrast, methionine is converted to methionine sulfoxide, which can be further oxidized to irreversible sulfone residues *via* the sequential addition of oxygen atoms. Being a hydrophobic amino acid, methionine residues establish hydrophobic bonds with the aromatic amino acids in the protein core. The strength of these hydrophobic bonds is equivalent to the bond energy of salt bridges and thereby provides structural stability to proteins (64). Oxidation of methionine causes the loss of hydrophobic bonds, and the buried hydrophobic amino acids of the protein get exposed to the cellular milieu, increasing the surface hydrophobicity of the protein, thereby compromising the integrity of the three-dimensional protein structure. As a result, oxidized proteins present an increased propensity to degradation (65). Consistent with this knowledge, we observe increased turnover of Atg19 and Ape1 proteins of the Cvt pathway during oxidative stress (Fig. 2*E*).

By reducing methionine sulfoxides to native methionines, Msrs neutralize oxidative damage. Prior reports in yeast show that deletion of *MXR1* leads to mitochondrial dysfunction (17). However, our earlier studies demonstrated that yeast cells devoid of *MXR2* are more susceptible to oxidative stress than that of *MXR1* and identified Mxr2 primarily as a mitochondrial matrix resident protein (52). We first identified mitochondrially localized yeast Mge1 as the first *in vivo* substrate of Mxr2 (51). Besides acting as a nucleotide exchange factor for Hsp70,

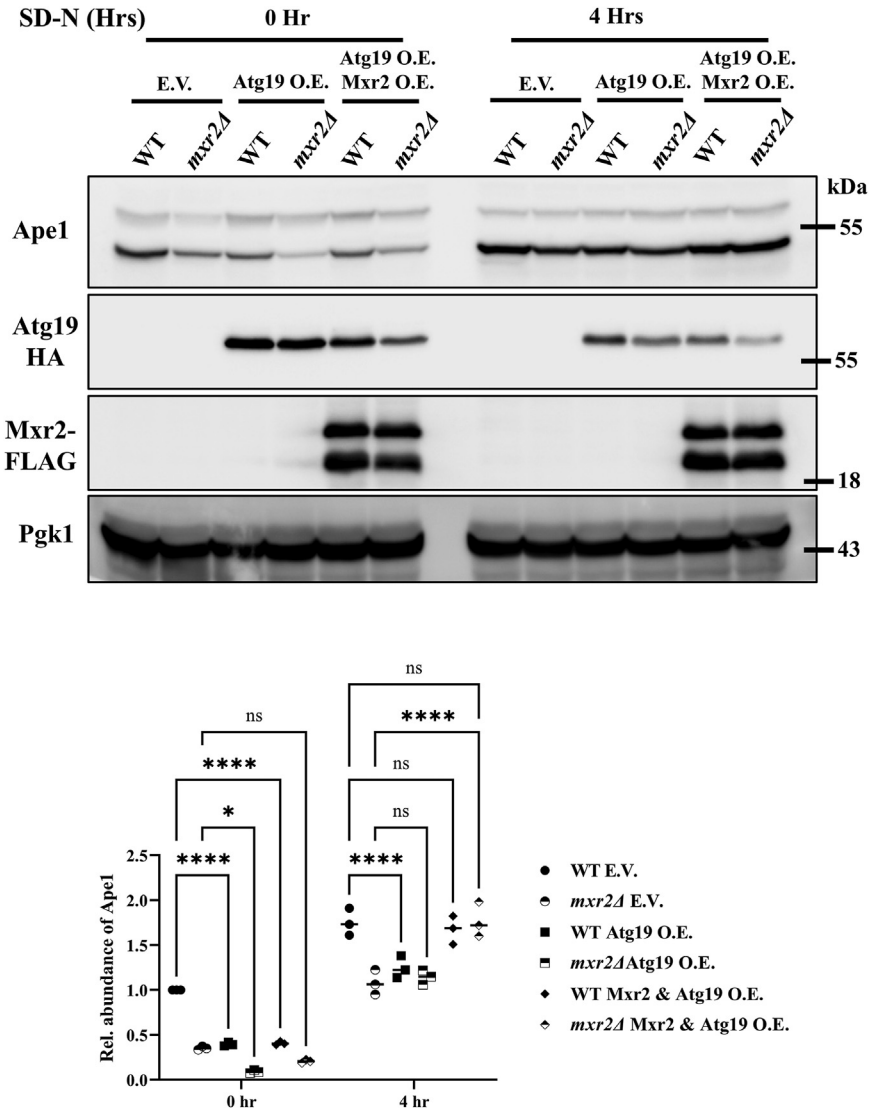

Figure 6. Mxr2 maintains stoichiometry of Atg19 and Ape1 in the Cvt pathway. wt and *mxr2*Δ cells carrying empty vectors or expressing either HA-Atg19 alone or with Flag-Mxr2 were grown up to the mid-log phase. Next, cells were exposed to nitrogen starvation for fourhours to induce oxidative stress or left untreated. Cells were harvested, lysed, and analyzed *via* immunoblotting with Ape1, HA, and FLAG antibodies. The data are represented as mean ± SD of three independent experiments and full-length blots are represented in Supporting information 2. Statistical analysis was done using a two-way ANOVA test. ****$p < 0.0001$, ***$p < 0.001$, **$p < 0.01$ and *$p < 0.05$. ns, nonsignificant. Cvt, cytoplasm to vacuole targeting; HA, hemagglutinin.

Mge1 is an oxidative stress sensor (66). Later, another study showed that the nucleotide exchange factor of cytosolic Hsp70, Fes1, is regulated by Mxr1 and Mxr2 *via* reversible methionine oxidation (53). Consistent with our earlier findings, this study also showed that Mxr2 is additionally present in the cytosol besides mitochondria (53). These earlier studies opened up the possibility of identification of other cytosolic substrates of Mxr2.

This study employs yeast two-hybrid and immunoprecipitation methods to identify novel cytosolic substrates for Mxr2. For the first time, we show that Mxr2 regulates two Cvt pathway proteins, Atg19 and Ape1 (Fig. 1). Deletion of MXR2 decreases the abundance of Ape1 and Atg19 without affecting their transcript levels (Fig. 2, *A* and *B*). The absence of Mxr2 has a more profound effect on the Ape1 protein level than Atg19 despite showing higher binding to Atg19 by two-hybrid analysis (Figs. 2*Ai* *versus* 2*Aii* *versus* 1*A*). Atg19 may be facilitating the interaction between Mxr2 and Ape1. Results from the cycloheximide chase assay depict the unstable nature of Ape1 in the absence of Mxr2 and its propensity to degradation. This result can be reconciled with our earlier finding that Δ*mxr2* cells are more susceptible to oxidative stress as they carry more ROS than wt cells grown in the presence or absence of nonfermentable carbon sources. This reasoning is confirmed when we observe the degradation of Ape1 and Atg19 in wt cells exposed to oxidative stress (Fig. 2). This study shows that the absence of Mxr2 or oxidative stress destabilizes the Cvt pathway proteins, Ape1 and Atg19 (Fig. 7). However, further studies are required to unravel the oxidative stress-induced structural alterations these proteins undergo.

Mxr2 interacts only with prApe1 and not processed Ape1 (Fig. 3). This result is substantiated by the finding that the interaction between Mxr2 and Ape1 is contingent on M17 alone, although Ape1 harbors more methionine (Fig. 3). It is

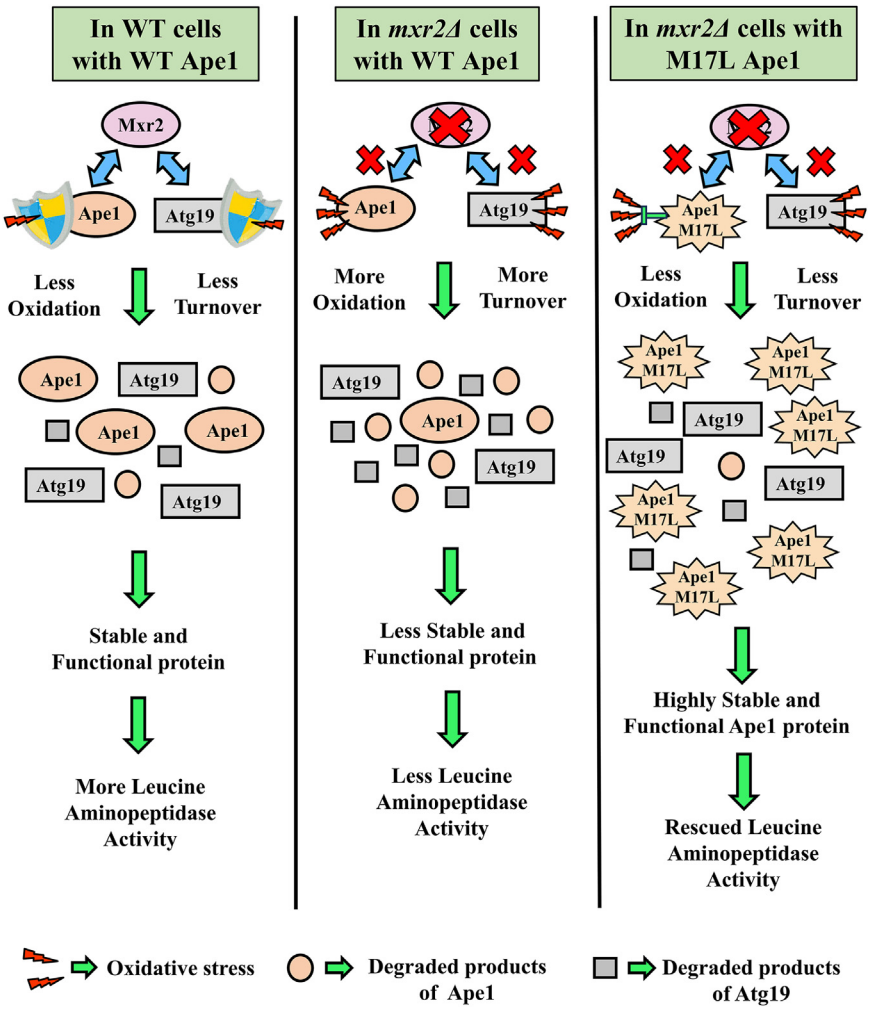

Figure 7. Schematic diagram depicting the role of Mxr2 in the Cvt pathway. (*Left panel*) In wt cells, Mxr2 interacts and protects Ape1 and Atg19 from oxidative stress, thereby preventing premature turnover. (*Middle panel*) Excess ROS in *mxr2*Δ cells destabilizes Ape1 and Atg19 proteins. Destabilized proteins tend to degrade faster, and in this context, leading to decreased leucine aminopeptidase activity. (*Right* panel) M17L mutation confers oxidative stress resistance to the Ape1 protein. Stable and oxidative stress-resistant Ape1 M17L protein rescues the decreased leucine aminopeptidase activity phenotype of the *mxr2*Δ strain. Cvt, cytoplasm to vacuole targeting; ROS, reactive oxygen species.

possible that prApe1 adopts a conformation where M17 is the only methionine susceptible to oxidation, making it mandatory to interact with Mxr2 for its reduction. Additionally, it shows that Mxr2 intervenes at a very early stage of the Cvt pathway when the proteins are more exposed to oxidative stress.

Msrs interact with oxidized methionine sulfoxides to reduce them to methionines. The catalytic mechanism was first elucidated on MsrA enzymes. It was later found that both MsrA and MsrB follow a canonical process where three cysteine residues from the enzymes participate in the reduction reaction (67). The first cysteine makes a nucleophilic attack on the sulfoxide moiety to form an unstable intermediate that breaks down to form sulfenic acid at the first cysteine, releasing a reduced methionine. The other two cysteines reduce the sulfenic acid at first cysteine residue by exchanging multiple thiol-disulfide reactions using the thioredoxin system and NADPH (15, 68–71).

Our earlier study identified Met155 within Mge1, which interacts with Mxr2. Substitution of this methionine with leucine disrupted the interaction between Mxr2 and Mge1 and made the protein more stable, conferring oxidative stress resistance to cells (52, 72).Mutation of methionine 17 to leucine in Ape1 renders it resistant to degradation (Figs. 4*C* and 7) and does not interact with Mxr2 (Fig. 3*C*); however, it does not affect its maturation. Met17 lies in the propeptide region of the Ape1 protein and plays a vital role in Ape1 assembly and interaction with Atg19. Structural analysis of the first 1 to 22 amino acids of Ape1 shows that this region comprises an α-helical structure adjacent to a flexible region. This α-helical region interacts with two other alpha helices to form an Ape1 trimer. Leu11 in the α-helices plays a crucial role as Leu11Ser mutation impairs Ape1 oligomerization and downstream processing (34). By characterizing another residue in the propeptide, Met17, in Ape1 stability and response to oxidative stress, we underscore the importance of Ape1 propeptide in the Cvt pathway. The identity of the methionine residues in Atg19 that interact with Mxr2 remains to be identified.

Vacuoles in yeast and lysosomes in higher eukaryotes serve as central multifunctional organelles. They store nutrient molecules, maintain metal ion homeostasis, and act as hubs for protein degradation by vacuolar proteases (73). In vegetative conditions, they are involved in 40% of total protein degradation during normal physiological conditions that can reach up to 85% during nutrient starvation (74). Compromised vacuolar or lysosomal-mediated protein degradation can cause physiological abnormalities, leading to many diseases. The Cvt pathway transports three vacuolar hydrolases: Ape1, Ams1, and Ape4, where Ape1 is a leucine aminopeptidase. We observe a significant reduction in LAP activity in the *mxr2*Δ strain compared to the wt strain (Fig. 5*B*). Curiously, the LAP activity of the *mxr2*Δ strain is comparable to that of the *ape1*Δ strain, suggesting that the residual Ape1 protein in *mxr2*Δ strain is not enzymatically efficient (Fig. 5). Given that Mxr2 interacts with only prApe1 and the level of mApe1 is reduced in *mxr2*Δ strain, the deletion of *MXR2* indirectly affects the activity of mApe1.

The Ape1 complex communicates with the autophagy machinery *via* Atg19. As the Ape1 maturation is abolished in the absence of Atg19 (Fig. 2*Ai*), we tried to rescue the instability phenotype of Ape1 in *the mxr2*Δ strain *via* overexpression of Atg19. Surprisingly, overexpression of Atg19 further destabilizes Ape1 in *the mxr2*Δ strain. Interestingly, overexpression of Atg19 in the wt strain has a dominant negative effect, possibly by overwhelming the antioxidant machinery and competing with Ape1 for binding to Mxr2 (Fig. 6). An imbalance in the stoichiometry of Mxr2 to Ape1 may occur in the wt strain when Atg19 is overexpressed, resulting in an accelerated turnover of Ape1 (Fig. 6). This assumption is vindicated when overexpression of Mxr2 nullifies the dominant negative effect of Atg19 overexpression in both wt and *mxr2*Δ strain robustly during nitrogen starvation and partially during normal physiological conditions. Based on these results, we conclude that the dependence of Ape1 and Atg19 proteins of the Cvt pathway on Mxr2 is critical for the operation of the Cvt pathway during oxidative stress.

Selective autophagy is involved in diverse vital physiological pathways, for example, secretory pathways, vesicular trafficking, and other intracellular transport processes (75). Impairment of selective autophagy has been well characterized in different clinical conditions like Alzheimer's and Parkinson's disease (76), chronic obstructive pulmonary disease (77), tuberculosis (78), HIV (79), and acute lung injury in hyperoxia (80). Cvt pathway has been depicted only in *S. cerevisiae* and *Pichia pastoris* and is not conserved through evolution (81). Nevertheless, it is one of the most characterized specific autophagy pathways. It serves as a model system to understand how particular cargos are selected, interact with the autophagy machinery, and get packed within the vesicle and delivered to the vacuole due to fewer molecular players and less cargo. Hence, investigating and elucidating the Cvt pathway and understanding its regulation will provide insights into other more complex autophagy pathways in higher eukaryotes. By identifying Atg19 and Ape1 as cytosolic substrates of Mxr2, we spotlight a hitherto unmapped link between two unrelated physiological machineries: the MSR system and the Cvt autophagy pathway.

Experimental procedures

Yeast strains and plasmids

The yeast strains used in this study are derived from the parent strain BY4741 and are listed in Table 1. Genomic deletion of the *MXR2* gene was achieved by replacing the ORF of the *MXR2* gene with HIS3MX6 cassette by PCR-based homologous recombination using NB1164/NB1165 primers, as indicated (82). For generating the plasmid constructs, the coding regions of the genes were amplified either from yeast genomic DNA or mentioned. All the plasmids and the primers are listed in Tables 2–4, respectively. To generate p425TEF Mxr2-FLAG, the coding region of *MXR2* was amplified using primers NB815/NB1048, where the reverse primer NB1048 has the 3× flag sequence embedded within it. The PCR product was then digested with BamHI/XhoI and ligated with digested p425TEF (pNB356) empty vector to create pNB904. MXR2-FLAG fragment from pNB904 was then subcloned into BamHI/SalI sites of yeast two-hybrid vector pGBD-C1(pNB415) to generate pNB901. For constructing yeast two-hybrid vectors pGAD-*APE1*, pGAD-*ATG19*, and pGBD-*MXR1*, the coding regions of *APE1*, *ATG19*, and *MXR1* genes were amplified using NB1364/NB1365, NB1362/NB1363, and NB 1678/NB1679, respectively and digested with ClaI/SalI, BamHI/SalI, and EcoRI/BamHI enzymes, respectively. Double-digested DNA fragments were ligated to the respective site of pGAD-C1 (pNB422) and pGBD-C1 to generate pNB902, pNB903, and pNB912, respectively. For producing the over-expressing constructs of *APE1* and *ATG19* with HA tag, DNA fragments of both genes were amplified using NB1404/NB1405 and NB1362/NB1399 primers, respectively, where both reverse primers (NB1405 and NB1399) have the HA tag sequence embedded within them. The amplified DNA fragments were then digested with HindIII/SalI and BamHI/XhoI enzymes, respectively, and then ultimately ligated to respective sites of p426 (pNB356) to generate pNB906 and pNB907. To create Δ45 deletion mutation of the first 45 amino acids in the *APE1* gene, the requisite DNA fragment was amplified using NB1563/NB1365 and ligated to ClaI/SalI sites of pGAD-C1 to generate pNB908. For creating further point mutations in *APE1* genes, at first *APE1* coding region was amplified with NB1645/NB1365 and NB 1633/NB1365 primers to create M1L single and M1L/M17L double mutation, respectively. After digesting the amplified fragments with ClaI/SalI, DNA fragments were then ligated to respective sites of pGAD-C1 to generate pNB911 and pNB909. For generating M17 single mutant, pNB909 was used as a template and amplified with NB1364/NB1365 primers and after digestion with ClaI/SalI, ligated to the same sites in pGAD-C1 vector to generate pNB910. For expressing wt and M17L *APE1* from the pRS315 CEN vector, 5′ UTR of the gene (380 bp) was amplified with NB1406/NB1674 primers and the coding region of the gene along with 3′ UTR (729 bp) was amplified with either NB1499/NB1511 (for wt *APE1*) or NB1675/NB1511 (for M17L *APE1*)

Table 1
Strains

Strain	Genotype	Reference
YNB105	BY4741; *MATa his3Δ1; leu2Δ0; met15Δ0; ura3Δ*	Euroscarf
YNB117	BY4741; *mxr2Δ::KANMX*	Euroscarf
YNB 339	PJ469-A	(87)
YNB 483	BY4741; *atg19Δ::KANMX*	Euroscarf
YNB 484	BY4741; *ape1Δ::KANMX*	Euroscarf
YNB 514	BY4741; ape1Δ::*KANMX* *mxr2Δ::HIS3*	This study

primers. The 5′ UTR and the gene along with 3′ UTR fragments were then digested with NotI/SpeI and SpeI/ApeI and then ligated to NotI/ApaI site of the pRS315 (pNB399) to generate pNB913 and pNB914. For the construction of pRS313 ATG19-HA, 5′ UTR of the gene (700 bp) and the DNA fragment having *ATG19* coding region along with HA tag were amplified using NB1400/NB1401 and NB1362/NB1399 primers, respectively. The amplified products after digestion with NotI/BamHI (5′ UTR) and BamHI/XhoI (gene sequence with HA tag) were then ligated to NotI/XhoI digested pRS313(pNB398) to generate pNB915.

Media and growth conditions

Yeast cells of the mid-log phase (A_{600} = approximately 0.8–1) were used for all experiments, where strains were grown at 30 °C either in synthetic medium with dextrose [0.67% yeast nitrogen base (Becton Dickinson, 291940), 2% dextrose (Himedia, GRM077), and supplemented auxotrophic amino acids and vitamins as needed, pH 5.5] as described previously (83) or in synthetic minimal medium, where specific auxotrophic nutrient needed for plasmid DNA selection in the experiment was not supplemented. To induce autophagic condition, where *APE1* expression increases, cells grown up to mid-log phase were incubated in nitrogen starvation medium [0.17% yeast nitrogen base having neither ammonium sulfate nor amino acids (Becton Dickinson, 233520), and 2% dextrose]. For imparting oxidative stress, cells from mid-log phase were treated with 2 mM H_2O_2 for 2 h at 30 °C. Yeast cell were transformed with plasmids using lithium acetate and single-stranded carrier DNA, as described (84). For yeast two hybrid analysis, transformants carrying yeast two hybrid constructs were grown, serially diluted, and spotted on selection plates and then incubated at 30 °C for 2 to 3 days, as described (85).

Table 2
Plasmids

Plasmid no.	Plasmid Name	Source/Reference
pNB478	pFA6a-HisMX6	(88)
pNB415	pGBD-C1	(87)
pNB422	pGAD-C1	(87)
pNB901	pGBD-C1 *MXR2-Flag*	This study
pNB902	pGAD-C1 *APE1*	This study
pNB903	pGAD-C1 *ATG19*	This study
pNB908	pGAD-C1 *APE1Δ45*	This study
pNB909	pGAD-C1 *APE1* DM (*M1L,M17L*)	This study
pNB910	pGAD-C1 *APE1 M17L*	This study
pNB911	pGAD-C1 *APE1 M1L*	This study
pNB912	pGBD-C1 *MXR1*	This study
pNB356	p425 TEF	(89)
pNB357	p426 TEF	(89)
pNB904	p425TEF *MXR2-Flag*	This study
pNB905	p426TEF *APE1-HA*	This study
pNB906	p426TEF *ATG19-HA*	This study
pNB270	p426TEF *MXR2-Flag*	(52)
pNB399	pRS315	(90)
pNB398	pRS313	(90)
pNB913	pRS315 *APE1*	This study
pNB914	pRS315 *APE1 M17L*	This study
pNB915	pRS313 *ATG19*	This study

Whole cell lysate preparation and immunoblotting

Yeast cells of A_{600nm} 3.0 were harvested and washed with water to prepare whole cell lysate. The washed cells were then resuspended in freshly prepared 200 µl lysis buffer [1.85 M NaOH (Himedia, MB095), 7.4% β-mercaptoethanol (Sigma-Aldrich, M3148)] and incubated on ice for 10 min. An equal volume of 50% trichloroacetic acid (Himedia, GRM6274) was then added to the cell suspension, mixed and incubated on ice for another 10 min. After incubation, the cell suspension was centrifuged at 13,000 R.P.M for 2 min at 4 °C. The protein pellet was then washed with 500 µl 1M Tris (Sigma-Aldrich, T6066) solution (not pH adjusted), without resuspending the pellet, by centrifugation at the same speed. The pellet was resuspended in 30 µl 1× Laemmli buffer and heated at 95 °C for 5 min. The protein samples were centrifuged at 13,000 RPM for 5 min after cooling down to collect the supernatant. Ten microliters of the supernatant, equivalent to 1 A_{600nm} cells, were then analyzed *via* SDS-PAGE. After electrophoresis, Western blot was performed following standard protocols. Immunoblotting was done with standard procedures with anti-FLAG antibody (Sigma-Aldrich, F3165, 1:2000), anti-HA antibody (Proteintech, 66006-2-Ig, 1:5000), anti-Pgk1 serum (kind gift from Prof. Debkumar Pain, New Jersey Medical School, Rutgers University), anti- Ape1 antibody (kind gift from Dr Claudine Kraft, Institute for Biochemistry and Molecular Biology, University of Freiburg), Horseradish peroxidase–conjugated anti-rabbit polyclonal antibody (Jackson Laboratories, 111-035-144, 1:25,000), anti-mouse polyclonal antibody (Jackson Laboratories, 115-035-146, 1:25,000). Immunoblotting signals enhanced by enhanced chemiluminescnce reagents (Advansta WesternBright, K-12045-D20) were detected in the Chemidoc imaging facility (Bio-Rad). Immunoblot images were quantified using Fiji software (http://imagej.net), followed by statistical analysis using GraphPad Prism8.

Coimmunoprecipitation

Cells, harvested for co-IP assay, were washed, and then resuspended in NP-40 lysis buffer [50 mM Tris–HCl buffer pH8, 150 mM NaCl (Himedia, GRM031), 2 mM EDTA (Amresco, 0105), 2 mM $MgCl_2$ (SRL, 69396), 1% NP-40 (Sigma-Aldrich, I8896), 1× Protease inhibitor cocktail (Roche, 04693132001)]. Resuspended cells were then lysed with glass beads using the bead-beating method. The cell lysate was centrifuged at 12,000 R.P.M. for 12 min to remove the cell debris and supernatant with soluble protein fraction was collected. After protein estimation with Lowry reagents, 1 mg of the supernatant was incubated with 10 µl of Protein

Table 3
Primers

Primer name	Sequence (5′-3′)	Restriction site	T_m
NB815 MXR2 fwd	ATCGGGATCCATGAATAAGTGGAGCAGGC	BamHI	62.9
NB1048 MXR2 FLAG rev	GTTTAAACCTCGAGTTACTTGTCATCGTCATCCTTGTAATCGA TGTCATGATCTTTATAATCACCGTCATGGTCTTTGTAGTCGGG CCCGTCGACATCCTTCTTGAGGTTTAAAGACGC	XhoI	77.2
NB1101 FLAG rev	ACATGTCGACTTACTTGTCATCGTCATCCTTGTAATCGATG	SalI	65.5
NB1164 Mxr2 deletion fwd	CCGATGATAGTTTAAATAAAGGGAGAAAGGAAGCA ATATCAAAAACGGATCCCCGGGTTAATTAA		69.7
NB1165 Mxr2 deletion rev	GTACGTATGCATACACACATATATATATATATATATATA GTACATGAATTCGAGCTCGTTTAAAC		65.9
NB1362 ATG19 fwd	CTAGGATCCATGAACAACTCAAAGACTAACC	BamHI	60.4
NB1363 ATG19 rev	ATGGTCGACGAGTTCTTCCCAAGTCAG	SalI	61.3
NB1364 APE1 fwd1	CCCATCGATATGGAGGAACAACGTGAAATAC	ClaI	61.7
NB1365 APE1 rev	ATGGTCGACCAACTCGCCGAATTCATC	SalI	61.3
NB1399 ATG19 HA rev	ATGCTCGAGCTAAGCATAATCTGGAACATCATATGGATAGT CGACGAGTTCTTCCCAAGTCAG	XhoI	72.4
NB1400 ATG19 5′ UTR fwd	CTAGCGGCCGCTGAGAAGCAATTGTGA	NotI	62.8
NB1401 ATG19 5′ UTR rev	ATGGGATCCTTACCAGAACTCTCCTTTGGG	BamHI	63
NB1404 APE1 fwd2	CTAAAGCTTATGGAGGAACAACGTGAAATAC	HindIII	59.1
NB1405 APE1 HA rev	ATGGTCGACCTAAGCATAATCTGGAACATCATATGGATA AGATCTCAACTCGCCGAATTCATC	SalI	71.1
NB1406 APE1 5′ UTR fwd	CTAGCGGCCGCGTCAGCTTCTACTTTAG	NotI	64.3
NB1499 APE1 fwd3	CCCACTAGTATGGAGGAACAACGTGAAATAC	SpeI	61.7
NB1511 APE1 3′ UTR rev	ATGGGGCCCCTTATTGCTTATTTGGCCC	ApaI	62.9
NB1563 APE1 Δ45 rev	CCCATCGATATGGAGCACAATTATGAGGATATTG	ClaI	62
NB1633 APE1 DM fwd	CCCATCGATCTGGAGGAACAACGTGAAATACTGGAACAATTG AAGAAAACTCTGCAGCTGCTAAC	ClaI	72.8
NB1645 APE1 M1L fwd	CCCATCGATCTGGAGGAACAACGTGAAATAC	ClaI	63
NB1674 APE1 5′ UTR rev	ATGACTAGTTCTTTTTTTCTTAATTTTGTTGGTTGTGC	SpeI	59.1
NB1675 APE1 M17L fwd	CCCACTAGTATGGAGGAACAACGTGAAATACTGGAACAATTG AAGAAAACTCTGCAGCTGCTAAC	SpeI	72.2
NB1678 MXR1 fwd	CTAGAATTCATGTCGTCGCTTATTTCAAAAACC	EcoRI	59.4
NB1679 MXR1 rev	ATGGGATCCCATTTCTCTCAGATAATGAGTA	BamHI	59.1
NB758 ACT1 RT fwd	GAAATCACCGCTTTGGCTCC		53.8
NB759 ACT1 RT rev	GTGGTGAACGATAGATGGACCA		54.8
NB1621 APE1 RT fwd	CGTCAACCACCTCTACAA		48
NB1622 APE1 RT rev	TGGCCATATGACCGTTAG		48
NB1623 ATG19 RT F P.-	TTACAGGCATCCCAAGAG		48
NB1624 ATG19 RT R P.- -	TGTCGTCACCGTCATAAG		48

A/G PLUS-Agarose beads (Santacruz Biotechnology, SC-2003) in an end-over-end rotator at 4 °C for 2 h, for pre-clearing step. The precleared supernatant was then incubated with anti-FLAG antibody at the same condition for overnight incubation. For binding of the antibody with the beads, 30 µl of protein A/G beads were added to the mix and again incubated at the same condition for 4 h. After incubation, beads were collected and washed three times with the lysis buffer and then analyzed *via* SDS-PAGE, followed by immunoblotting with anti-FLAG, anti-HA and anti-APE1 antibodies.

Table 4
GenBank Accession numbers of the genes used and expected size of the amplicons

MXR2 gene (GenBank Accession number - NM_001178678.1)	
Amplicon Name	Size in bp
Mxr2-3X FLAG	608
MXR2 deletion cassette	1403
APE1 Gene (GenBank Accession number - NM_001179669.1)	
Amplicon Name	Size in bp
APE1	1560
Δ(2–45) APE1	1431
APE1-HA	1596
APE1 with 5′ and 3′ UTR	2674
APE1 amplicon size in RT PCR	110
ATG19 Gene (GenBank Accession number - NM_001183336.1)	
Amplicon Name	Size in bp
ATG19	1263
ATG19-HA	1299
ATG19 with 5′ UTR	2010
Atg19 amplicon size in RT PCR	110

Cycloheximide chase assay

For the cycloheximide chase assay, strains were grown up to mid-log phase either in synthetic complete medium or synthetic minimal medium, as required, and then harvested. Harvested cells were then subjected to cycloheximide [Sigma-Aldrich, C7698] treatment (50 or 100 µg/ml) for different durations (0, 10, 30, 60, and 120 min). After each time point, cells were harvested and subjected to whole cell lysate preparation followed by the analysis of the protein degradation profile by immunoblotting with anti-Ape1 antibody.

RNA extraction, cDNA synthesis, and qRT-PCR

For RNA extraction, cells were harvested after growing up to mid-log phase. Total RNA was extracted using the hot acid phenol method described in (86). To remove DNA contamination, extracted RNA was subjected to DNase digestion, where 3 µg of RNA was incubated with 1 Unit of DNase I (Thermo Fisher Scientific, EN0521) at 37 °C for 2 h followed by DNase inactivation by incubating the mix with EDTA at 65 °C for 2 min. DNase treated RNA was subjected to complementary DNA (cDNA) synthesis using Verso cDNA Synthesis Kit (Thermo Fisher Scientific, AB1453A) as per kit protocol, where 1 µg of RNA was used and incubated at 42 °C for 35 min followed by inactivation at 95 °C for 2 min, along with the kit reagents. One µg of cDNA was diluted to a final concentration of 40 ng/µl, and 1 µl of cDNA was analyzed *via*

qRT-PCR in a final volume of 10 µl reaction mix with the PowerUp SYBR Green PCR Master mix (Applied Biosystems, A25742) using a Quanstudio 3 Real-Time PCR System.

LAP assay

For LAP activity assay, the respective strains were grown in minimal medium up to mid log phase and harvested. Cell lysates were prepared using lysis buffer previously described for performing co-immunoprecipitation. Fifty micrograms of cell lysate was used for each reaction. A total volume of 500 µl of reaction mixture were prepared consisting of 400 µl of 75 mM Tris–HCl pH-7.5, 50 µl 20 mM leucine para nitroanilide (Sigma-Aldrich, L9125) and 50 µg of cell lysate and incubated at 30 °C for 15, 30, and 45 min time points. After incubation, spectrophotometric analysis was performed at 405 nm and µmol of product formed/mg of cell lysate was calculated according to the equation mentioned in Figure 5*B*.

Data availability

The manuscript contains all the data.

Supporting information—This article contains Supporting information.

Acknowledgments—The authors thank Dr Krishnaveni Mishra (Department of Biochemistry, University of Hyderabad) for yeast deletion strains, and pRS313 and pRS315 plasmids, and Dr EA. Craig (Department of Biochemistry, University of Wisconsin–Madison) for yeast-two-hybrid plasmids and strains. The authors also thank Dr Claudine Kraft (Institute for Biochemistry and Molecular Biology, University of Freiburg) for the Ape1 antibody and Dr Debkumar Pain (New Jersey Medical School, Rutgers University) for the Pgk1 antibody. The authors thank Dr Thanuja Krishnamoorthy, Vectrogen Biologicals, India, for her input and editing of the article. A. C acknowledges SRF & JRF fellowships from CSIR, India.

Author contributions—A. C. and N. B. V. S. methodology; A. C. and N. B. V. S. writing–original draft; A. C. investigation; N. B. V. S. supervision; N. B. V. S. funding acquisition.

Funding and additional information—Funds from DST-FST to the Department, DBT-Builder to the School of Life Sciences, and UOH-IOE and CSIR, India (37/1747/23/EMR-II) grants to N. B. V. S. supported this study.

Conflict of interest—The authors declare that they have no conflict of interest with the contents of this article.

Abbreviations—The abbreviations used are: Cvt, cytoplasm to vacuole targeting; HA, hemagglutinin; LAP, leucine aminopeptidase; MSR, methionine sulfoxide reductase; PAS, phagophore assembly site; ROS, reactive oxygen species; qRT-PCR, quantitative reverse transcription PCR.

References

1. Nathan, C. (2003) Specificity of a third kind: reactive oxygen and nitrogen intermediates in cell signaling. *J. Clin. Invest.* **111**, 769–778
2. D'Autréaux, B., and Toledano, M. B. (2007) ROS as signalling molecules: mechanisms that generate specificity in ROS homeostasis. *Nat. Rev. Mol. Cell Biol.* **8**, 813–824
3. Imlay, J. A. (2003) Pathways of oxidative damage. *Annu. Rev. Microbiol.* **57**, 395–418
4. Stadtman, E. R., and Berlett, B. S. (1998) Reactive oxygen-mediated protein oxidation in aging and disease. *Drug Metab. Rev.* **30**, 225–243
5. Anjum, N. A., Sofo, A., Scopa, A., Roychoudhury, A., Gill, S. S., Iqbal, M., *et al.* (2015) Lipids and proteins–major targets of oxidative modifications in abiotic stressed plants. *Environ. Sci. Pollut. Res. Int.* **22**, 4099–4121
6. Birben, E., Sahiner, U. M., Sackesen, C., Erzurum, S., and Kalayci, O. (2012) Oxidative stress and antioxidant defense. *World Allergy Organ J.* **5**, 9–19
7. Levine, R. L., Moskovitz, J., and Stadtman, E. R. (2000) Oxidation of methionine in proteins: roles in antioxidant defense and cellular regulation. *IUBMB Life* **50**, 301–307
8. Brot, N., and Weissbach, H. (1991) Biochemistry of methionine sulfoxide residues in proteins. *Biofactors* **3**, 91–96
9. Stadtman, E. R., Moskovitz, J., Berlett, B. S., and Levine, R. L. (2002) Cyclic oxidation and reduction of protein methionine residues is an important antioxidant mechanism. *Mol. Cell Biochem.* **234-235**, 3–9
10. Kim, H. Y., and Gladyshev, V. N. (2005) Role of structural and functional elements of mouse methionine-S-sulfoxide reductase in its subcellular distribution. *Biochemistry* **44**, 8059–8067
11. Zhang, X. H., and Weissbach, H. (2008) Origin and evolution of the protein-repairing enzymes methionine sulphoxide reductases. *Biol. Rev. Camb Philos. Soc.* **83**, 249–257
12. Weissbach, H., Etienne, F., Hoshi, T., Heinemann, S. H., Lowther, W. T., Matthews, B., *et al.* (2002) Peptide methionine sulfoxide reductase: structure, mechanism of action, and biological function. *Arch. Biochem. Biophys.* **397**, 172–178
13. Tarrago, L., Kaya, A., Weerapana, E., Marino, S. M., and Gladyshev, V. N. (2012) Methionine sulfoxide reductases preferentially reduce unfolded oxidized proteins and protect cells from oxidative protein unfolding. *J. Biol. Chem.* **287**, 24448–24459
14. Boschi-Muller, S., Gand, A., and Branlant, G. (2008) The methionine sulfoxide reductases: catalysis and substrate specificities. *Arch. Biochem. Biophys.* **474**, 266–273
15. Lowther, W. T., Brot, N., Weissbach, H., Honek, J. F., and Matthews, B. W. (2000) Thiol-disulfide exchange is involved in the catalytic mechanism of peptide methionine sulfoxide reductase. *Proc. Natl. Acad. Sci. U. S. A.* **97**, 6463–6468
16. Neiers, F., Kriznik, A., Boschi-Muller, S., and Branlant, G. (2004) Evidence for a new sub-class of methionine sulfoxide reductases B with an alternative thioredoxin recognition signature. *J. Biol. Chem.* **279**, 42462–42468
17. Kaya, A., Koc, A., Lee, B. C., Fomenko, D. E., Rederstorff, M., Krol, A., *et al.* (2010) Compartmentalization and regulation of mitochondrial function by methionine sulfoxide reductases in yeast. *Biochemistry* **49**, 8618–8625
18. Le, D. T., Lee, B. C., Marino, S. M., Zhang, Y., Fomenko, D. E., Kaya, A., *et al.* (2009) Functional analysis of free methionine-R-sulfoxide reductase from Saccharomyces cerevisiae. *J. Biol. Chem.* **284**, 4354–4364
19. Taggart, C., Cervantes-Laurean, D., Kim, G., McElvaney, N. G., Wehr, N., Moss, J., and Levine, R. L. (2000) Oxidation of either methionine 351 or methionine 358 in alpha 1-antitrypsin causes loss of anti-neutrophil elastase activity. *J. Biol. Chem.* **275**, 27258–27265
20. Panzenböck, U., and Stocker, R. (2005) Formation of methionine sulfoxide-containing specific forms of oxidized high-density lipoproteins. *Biochim. Biophys. Acta* **1703**, 171–181
21. Brennan, L. A., Lee, W., Cowell, T., Giblin, F., and Kantorow, M. (2009) Deletion of mouse MsrA results in HBO-induced cataract: MsrA repairs mitochondrial cytochrome c. *Mol. Vis.* **15**, 985–999
22. Gabbita, S. P., Aksenov, M. Y., Lovell, M. A., and Markesbery, W. R. (1999) Decrease in peptide methionine sulfoxide reductase in Alzheimer's disease brain. *J. Neurochem.* **73**, 1660–1666
23. Glaser, C. B., Yamin, G., Uversky, V. N., and Fink, A. L. (2005) Methionine oxidation, alpha-synuclein and Parkinson's disease. *Biochim. Biophys. Acta* **1703**, 157–169

24. Bleackley, M. R., Young, B. P., Loewen, C. J. R., and MacGillivray, R. T. A. (2011) High density array screening to identify the genetic requirements for transition metal tolerance in Saccharomyces cerevisiae. *Metallomics* **3**, 195–205
25. Baba, M., Osumi, M., Scott, S. V., Klionsky, D. J., and Ohsumi, Y. (1997) Two distinct pathways for targeting proteins from the cytoplasm to the vacuole/lysosome. *J. Cell Biol.* **139**, 1687–1695
26. Scott, S. V., Baba, M., Ohsumi, Y., and Klionsky, D. J. (1997) Aminopeptidase I is targeted to the vacuole by a nonclassical vesicular mechanism. *J. Cell Biol.* **138**, 37–44
27. Lynch-Day, M. A., and Klionsky, D. J. (2010) The Cvt pathway as a model for selective autophagy. *FEBS Lett.* **584**, 1359–1366
28. Umekawa, M., and Klionsky, D. J. (2012) The cytoplasm-to-vacuole targeting pathway: a historical perspective. *Int. J. Cell Biol.* **2012**, 142634
29. Kim, J., Scott, S. V., Oda, M. N., and Klionsky, D. J. (1997) Transport of a large oligomeric protein by the cytoplasm to vacuole protein targeting pathway. *J. Cell Biol.* **137**, 609–618
30. Shintani, T., and Klionsky, D. J. (2004) Cargo proteins facilitate the formation of transport vesicles in the cytoplasm to vacuole targeting pathway. *J. Biol. Chem.* **279**, 29889–29894
31. Oda, M. N., Scott, S. V., Hefner-Gravink, A., Caffarelli, A. D., and Klionsky, D. J. (1996) Identification of a cytoplasm to vacuole targeting determinant in aminopeptidase I. *J. Cell Biol.* **132**, 999–1010
32. Scott, S. V., Guan, J., Hutchins, M. U., Kim, J., and Klionsky, D. J. (2001) Cvt19 is a receptor for the cytoplasm-to-vacuole targeting pathway. *Mol. Cell* **7**, 1131–1141
33. Shintani, T., Huang, W. P., Stromhaug, P. E., and Klionsky, D. J. (2002) Mechanism of cargo selection in the cytoplasm to vacuole targeting pathway. *Dev. Cell* **3**, 825–837
34. Yamasaki, A., Watanabe, Y., Adachi, W., Suzuki, K., Matoba, K., Kirisako, H., *et al.* (2016) Structural basis for receptor-mediated selective autophagy of aminopeptidase I aggregates. *Cell Rep.* **16**, 19–27
35. Morales Quinones, M., Winston, J. T., and Stromhaug, P. E. (2012) Propeptide of aminopeptidase 1 protein mediates aggregation and vesicle formation in cytoplasm-to-vacuole targeting pathway. *J. Biol. Chem.* **287**, 10121–10133
36. Sawa-Makarska, J., Abert, C., Romanov, J., Zens, B., Ibiricu, I., and Martens, S. (2014) Cargo binding to Atg19 unmasks additional Atg8 binding sites to mediate membrane-cargo apposition during selective autophagy. *Nat. Cell Biol.* **16**, 425–433
37. Hutchins, M. U., and Klionsky, D. J. (2001) Vacuolar localization of oligomeric alpha-mannosidase requires the cytoplasm to vacuole targeting and autophagy pathway components in Saccharomyces cerevisiae. *J. Biol. Chem.* **276**, 20491–20498
38. Suzuki, K., Kondo, C., Morimoto, M., and Ohsumi, Y. (2010) Selective transport of alpha-mannosidase by autophagic pathways: identification of a novel receptor, Atg34p. *J. Biol. Chem.* **285**, 30019–30025
39. Watanabe, Y., Noda, N. N., Kumeta, H., Suzuki, K., Ohsumi, Y., and Inagaki, F. (2010) Selective transport of alpha-mannosidase by autophagic pathways: structural basis for cargo recognition by Atg19 and Atg34. *J. Biol. Chem.* **285**, 30026–30033
40. Yuga, M., Gomi, K., Klionsky, D. J., and Shintani, T. (2011) Aspartyl aminopeptidase is imported from the cytoplasm to the vacuole by selective autophagy in Saccharomyces cerevisiae. *J. Biol. Chem.* **286**, 13704–13713
41. Yorimitsu, T., and Klionsky, D. J. (2005) Atg11 links cargo to the vesicle-forming machinery in the cytoplasm to vacuole targeting pathway. *Mol. Biol. Cell* **16**, 1593–1605
42. Reggiori, F., Monastyrska, I., Shintani, T., and Klionsky, D. J. (2005) The actin cytoskeleton is required for selective types of autophagy, but not nonspecific autophagy, in the yeast Saccharomyces cerevisiae. *Mol. Biol. Cell* **16**, 5843–5856
43. Monastyrska, I., Reggiori, F., and Klionsky, D. J. (2008) Harpooning the Cvt complex to the phagophore assembly site. *Autophagy* **4**, 914–916
44. Geng, J., and Klionsky, D. J. (2008) Quantitative regulation of vesicle formation in yeast nonspecific autophagy. *Autophagy* **4**, 955–957
45. Noda, N. N., Kumeta, H., Nakatogawa, H., Satoo, K., Adachi, W., Ishii, J., *et al.* (2008) Structural basis of target recognition by Atg8/LC3 during selective autophagy. *Genes Cells* **13**, 1211–1218
46. Reggiori, F., and Klionsky, D. J. (2006) Atg9 sorting from mitochondria is impaired in early secretion and VFT-complex mutants in Saccharomyces cerevisiae. *J. Cell Sci.* **119**, 2903–2911
47. Reggiori, F., Wang, C. W., Stromhaug, P. E., Shintani, T., and Klionsky, D. J. (2003) Vps51 is part of the yeast Vps fifty-three tethering complex essential for retrograde traffic from the early endosome and Cvt vesicle completion. *J. Biol. Chem.* **278**, 5009–5020
48. Kirisako, T., Ichimura, Y., Okada, H., Kabeya, Y., Mizushima, N., Yoshimori, T., *et al.* (2000) The reversible modification regulates the membrane-binding state of Apg8/Aut7 essential for autophagy and the cytoplasm to vacuole targeting pathway. *J. Cell Biol.* **151**, 263–276
49. Epple, U. D., Suriapranata, I., Eskelinen, E. L., and Thumm, M. (2001) Aut5/Cvt17p, a putative lipase essential for disintegration of autophagic bodies inside the vacuole. *J. Bacteriol.* **183**, 5942–5955
50. Teter, S. A., Eggerton, K. P., Scott, S. V., Kim, J., Fischer, A. M., and Klionsky, D. J. (2001) Degradation of lipid vesicles in the yeast vacuole requires function of Cvt17, a putative lipase. *J. Biol. Chem.* **276**, 2083–2087
51. Klionsky, D. J., Cueva, R., and Yaver, D. S. (1992) Aminopeptidase I of Saccharomyces cerevisiae is localized to the vacuole independent of the secretory pathway. *J. Cell Biol.* **119**, 287–299
52. Allu, P. K., Marada, A., Boggula, Y., Karri, S., Krishnamoorthy, T., and Sepuri, N. B. V. (2015) Methionine sulfoxide reductase 2 reversibly regulates Mge1, a cochaperone of mitochondrial Hsp70, during oxidative stress. *Mol. Biol. Cell* **26**, 406–419
53. Nicklow, E. E., and Sevier, C. S. (2020) Activity of the yeast cytoplasmic Hsp70 nucleotide-exchange factor Fes1 is regulated by reversible methionine oxidation. *J. Biol. Chem.* **295**, 552–569
54. Allu, P. K., Boggula, Y., Karri, S., Marada, A., Krishnamoorthy, T., and Sepuri, N. B. V. (2018) A conserved R type Methionine Sulfoxide Reductase reverses oxidized GrpEL1/Mge1 to regulate Hsp70 chaperone cycle. *Sci. Rep.* **8**, 2716
55. Yu, H., Braun, P., Yildirim, M. A., Lemmens, I., Venkatesan, K., Sahalie, J., *et al.* (2008) High-quality binary protein interaction map of the yeast interactome network. *Science* **322**, 104–110
56. Müller, M., Schmidt, O., Angelova, M., Faserl, K., Weys, S., Kremser, L., *et al.* (2015) The coordinated action of the MVB pathway and autophagy ensures cell survival during starvation. *Elife* **4**, e07736
57. Seguí-Real, B., Martinez, M., and Sandoval, I. V. (1995) Yeast aminopeptidase I is post-translationally sorted from the cytosol to the vacuole by a mechanism mediated by its bipartite N-terminal extension. *EMBO J.* **14**, 5476–5484
58. Brot, N., Weissbach, L., Werth, J., and Weissbach, H. (1981) Enzymatic reduction of protein-bound methionine sulfoxide. *Proc. Natl. Acad. Sci. U. S. A.* **78**, 2155–2158
59. Frey, J., and Röhm, K. H. (1978) Subcellular localization and levels of aminopeptidases and dipeptidase in Saccharomyces cerevisiae. *Biochim. Biophys. Acta* **527**, 31–41
60. Metz, G., and Röhm, K. H. (1976) Yeast aminopeptidase I. Chemical composition and catalytic properties. *Biochim. Biophys. Acta* **429**, 933–949
61. Trumbly, R. J., and Bradley, G. (1983) Isolation and characterization of aminopeptidase mutants of Saccharomyces cerevisiae. *J. Bacteriol.* **156**, 36–48
62. Schu, P. (2008) Aminopeptidase I enzymatic activity. *Methods Enzymol.* **451**, 67–78
63. Simonian, N. A., and Coyle, J. T. (1996) Oxidative stress in neurodegenerative diseases. *Annu. Rev. Pharmacol. Toxicol.* **36**, 83–106
64. Valley, C. C., Cembran, A., Perlmutter, J. D., Lewis, A. K., Labello, N. P., Gao, J., and Sachs, J. N. (2012) The methionine-aromatic motif plays a unique role in stabilizing protein structure. *J. Biol. Chem.* **287**, 34979–34991
65. Chao, C. C., Ma, Y. S., and Stadtman, E. R. (1997) Modification of protein surface hydrophobicity and methionine oxidation by oxidative systems. *Proc. Natl. Acad. Sci. U. S. A.* **94**, 2969–2974
66. Marada, A., Allu, P. K., Murari, A., PullaReddy, B., Tammineni, P., Thiriveedi, V. R., *et al.* (2013) Mge1, a nucleotide exchange factor of Hsp70, acts as an oxidative sensor to regulate mitochondrial Hsp70 function. *Mol. Biol. Cell* **24**, 692–703

67. Lowther, W. T., Weissbach, H., Etienne, F., Brot, N., and Matthews, B. W. (2002) The mirrored methionine sulfoxide reductases of Neisseria gonorrhoeae pilB. *Nat. Struct. Biol.* **9**, 348–352
68. Lowther, W. T., Brot, N., Weissbach, H., and Matthews, B. W. (2000) Structure and mechanism of peptide methionine sulfoxide reductase, an "anti-oxidation" enzyme. *Biochemistry* **39**, 13307–13312
69. Moskovitz, J., Poston, J. M., Berlett, B. S., Nosworthy, N. J., Szczepanowski, R., and Stadtman, E. R. (2000) Identification and characterization of a putative active site for peptide methionine sulfoxide reductase (MsrA) and its substrate stereospecificity. *J. Biol. Chem.* **275**, 14167–14172
70. Boschi-Muller, S., Azza, S., Sanglier-Cianferani, S., Talfournier, F., Van Dorsselear, A., and Branlant, G. (2000) A sulfenic acid enzyme intermediate is involved in the catalytic mechanism of peptide methionine sulfoxide reductase from Escherichia coli. *J. Biol. Chem.* **275**, 35908–35913
71. Tête-Favier, F., Cobessi, D., Boschi-Muller, S., Azza, S., Branlant, G., and Aubry, A. (2000) Crystal structure of the Escherichia coli peptide methionine sulphoxide reductase at 1.9 A resolution. *Structure* **8**, 1167–1178
72. Karri, S., Singh, S., Paripati, A. K., Marada, A., Krishnamoorthy, T., Guruprasad, L., *et al.* (2019) Adaptation of Mge1 to oxidative stress by local unfolding and altered Interaction with mitochondrial Hsp70 and Mxr2. *Mitochondrion* **46**, 140–148
73. Li, S. C., and Kane, P. M. (2009) The yeast lysosome-like vacuole: endpoint and crossroads. *Biochim. Biophys. Acta* **1793**, 650–663
74. Teichert, U., Mechler, B., Müller, H., and Wolf, D. H. (1989) Lysosomal (vacuolar) proteinases of yeast are essential catalysts for protein degradation, differentiation, and cell survival. *J. Biol. Chem.* **264**, 16037–16045
75. Stolz, A., Ernst, A., and Dikic, I. (2014) Cargo recognition and trafficking in selective autophagy. *Nat. Cell Biol.* **16**, 495–501
76. Youle, R. J., and Narendra, D. P. (2011) Mechanisms of mitophagy. *Nat. Rev. Mol. Cell Biol.* **12**, 9–14
77. Mizumura, K., Cloonan, S. M., Nakahira, K., Bhashyam, A. R., Cervo, M., Kitada, T., *et al.* (2014) Mitophagy-dependent necroptosis contributes to the pathogenesis of COPD. *J. Clin. Invest.* **124**, 3987–4003
78. Vergne, I., Chua, J., Singh, S. B., and Deretic, V. (2004) Cell biology of mycobacterium tuberculosis phagosome. *Annu. Rev. Cell Dev. Biol.* **20**, 367–394
79. Campbell, G. R., and Spector, S. A. (2012) Vitamin D inhibits human immunodeficiency virus type 1 and Mycobacterium tuberculosis infection in macrophages through the induction of autophagy. *PLoS Pathog.* **8**, e1002689
80. Liang, X., Wei, S. Q., Lee, S. J., Fung, J. K., Zhang, M., Tanaka, A., *et al.* (2013) p62 sequestosome 1/light chain 3b complex confers cytoprotection on lung epithelial cells after hyperoxia. *Am. J. Respir. Cell Mol. Biol.* **48**, 489–496
81. Meijer, W. H., van der Klei, I. J., Veenhuis, M., and Kiel, J. A. K. W. (2007) ATG genes involved in non-selective autophagy are conserved from yeast to man, but the selective Cvt and pexophagy pathways also require organism-specific genes. *Autophagy* **3**, 106–116
82. Longtine, M. S., McKenzie, A., Demarini, D. J., Shah, N. G., Wach, A., Brachat, A., *et al.* (1998) Additional modules for versatile and economical PCR-based gene deletion and modification in Saccharomyces cerevisiae. *Yeast* **14**, 953–961
83. Sherman, F. (1991) Getting started with yeast. *Methods Enzymol.* **194**, 3–21
84. Gietz, R. D., and Woods, R. A. (2002) Transformation of yeast by lithium acetate/single-stranded carrier DNA/polyethylene glycol method. *Methods Enzymol.* **350**, 87–96
85. Pal, A., Paripati, A. K., Deolal, P., Chatterjee, A., Prasad, P. R., Adla, P., and Sepuri, N. B. V. (2022) Eisosome protein Pil1 regulates mitochondrial morphology, mitophagy, and cell death in Saccharomyces cerevisiae. *J. Biol. Chem.* **298**, 102533
86. Collart, M. A., and Oliviero, S. (2001) Preparation of yeast RNA. *Curr. Protoc. Mol. Biol.* **Chapter 13**: p. Unit13.12
87. Büttner, S., Eisenberg, T., Carmona-Gutierrez, D., Ruli, D., Knauer, H., Ruckenstuhl, C., *et al.* (2007) Endonuclease G regulates budding yeast life and death. *Mol. Cell* **25**, 233–246
88. Moreira, K. E., Schuck, S., Schrul, B., Fröhlich, F., Moseley, J. B., Walther, T. C., and Walter, P. (2012) Seg1 controls eisosome assembly and shape. *J. Cell Biol.* **198**, 405–420
89. Mumberg, D., Müller, R., and Funk, M. (1995) Yeast vectors for the controlled expression of heterologous proteins in different genetic backgrounds. *Gene* **156**, 119–122
90. Sikorski, R. S., and Hieter, P. (1989) A system of shuttle vectors and yeast host strains designed for efficient manipulation of DNA in Saccharomyces cerevisiae. *Genetics* **122**, 19–27